



# Design and mechanism exploration of single-crystalline NCM811 materials with superior comprehensive performance for Li-ion batteries

Xiangbang Kong, Huiya Yang, Yige Zhang, Pengpeng Dai, Yonglin Tang, Jing Zeng<sup>\*</sup>, Jinbao Zhao<sup>\*</sup>

College of Chemistry and Chemical Engineering, State-Province Joint Engineering Laboratory of Power Source Technology for New Energy Vehicle, State Key Laboratory of Physical Chemistry of Solid Surfaces, Engineering Research Center of Electrochemical Technology, Ministry of Education, Collaborative Innovation Center of Chemistry for Energy Materials, Xiamen University, Xiamen 361005, PR China

## ARTICLE INFO

### Keywords:

Lithium-ion battery  
 $\text{LiNi}_x\text{Co}_y\text{Mn}_{1-x-y}\text{O}_2$   
 Single-crystalline  
 Doping modification  
 Electrochemical performance  
 Thermal stability

## ABSTRACT

Although single-crystalline  $\text{LiNi}_x\text{Co}_y\text{Mn}_{1-x-y}\text{O}_2$  (SC NCM) materials have been confirmed to have advantages in cycle performance, storage performance and thermal stability, the comprehensive performance of SC NCM materials is not perfect enough nowadays. And the current research on the modification mostly focuses on polycrystalline NCM materials, the modification of SC NCM materials is rare. Therefore, the synthesis and modification of SC NCM materials deserve special attention. In this work, the SC high-nickel  $\text{LiNi}_{0.8}\text{Co}_{0.1}\text{Mn}_{0.1}\text{O}_2$  (NCM811) is modified by doping with titanium (Ti) element. The doped material can maintain better structural stability, and suppress the side reaction between the material interface and the electrolyte, so the cycling performance is significantly improved. Doping enlarges the transport channel of  $\text{Li}^+$  in the material, thereby increasing the rate property. The lattice slip phenomenon of the modified material under high voltage is significantly suppressed, and the oxygen release and the reactivity with the electrolyte at high temperature of the material after delithiation are reduced, so the high voltage resistance and thermal stability are significantly enhanced. In conclusion, the comprehensive properties of SC NCM811 materials are improved by doping, and detailed mechanism study is carried out, which can provide reference for the further modification of SC NCM materials.

## 1. Introduction

As lithium-ion battery powered vehicles have become more and more popular in the market in recent years, consumers' demand for mileage of electric vehicles is also growing [1–3]. For lithium-ion batteries, the commonly used anode materials are generally graphite or silicon-based anode materials with a specific capacity of hundreds or thousands of milliamp hours per gram [4–6], but today's cathode materials can often provide a capacity of about  $200 \text{ mAh}\cdot\text{g}^{-1}$  [7,8]. Therefore, cathode materials are the key materials that determine the overall energy density of the batteries. Among them, NCM materials have attracted widespread attention because of their excellent comprehensive performance [9]. Their high specific capacity and low comprehensive cost have made important contributions to the progress of electric vehicle power batteries [10,11]. However, NCM materials are generally obtained by calcining the precursors formed by coprecipitation, and the NCM materials are often secondary particles

grown by the accumulation of primary particles [12,13]. Because of this characteristic, there are many inevitable inherent problems such as particle crushing and pulverization, interstitial deterioration and other problems [14–18]. The SC NCM materials are independent primary particles, and there is no particle gap, so it is significantly improved in many aspects compared with conventional polycrystalline NCM materials. For example, the SC NCM materials often show better cycle and storage performance and thermal stability [19–21]. However, the performance of the current SC NCM materials is not perfect enough due to limitations of synthetic methods [22–25], the particle shapes and sizes of many SC NCM materials are non-uniform, which affects the electrochemical performance. Smaller particle sizes increase the side reactions of SC NCM materials with the electrolyte, and the sharp particle morphology is more likely to be broken during the compaction process. Moreover, the current research on the modification of NCM materials mostly focuses on polycrystalline NCM materials [26,27], and the amendment of SC NCM materials is rare. Therefore, the research on the

<sup>\*</sup> Corresponding authors.

E-mail addresses: [zengjing@xmu.edu.cn](mailto:zengjing@xmu.edu.cn) (J. Zeng), [jbzha@xmu.edu.cn](mailto:jbzha@xmu.edu.cn) (J. Zhao).

<https://doi.org/10.1016/j.cej.2022.139431>

Received 16 August 2022; Received in revised form 21 September 2022; Accepted 22 September 2022

Available online 26 September 2022

1385-8947/© 2022 Published by Elsevier B.V.

synthesis and modification of SC NCM materials deserves researchers' attention.

In this work, a high-nickel single-crystalline NCM811 material with regular morphology and uniform particles is synthesized by the molten-salt method, and the comprehensive properties of the SC NCM material are further improved by Ti doping. Through the experimental research, it is found that the electrochemical performance and thermal stability of the modified material are obviously better than that of the unmodified original material. The stabilizing effect of Ti can enhance the structural stability of SC NCM811 during the electrochemical process and reduce the generation of surface impurities. Larger radius of Ti increases the interlayer spacing for  $\text{Li}^+$  diffusion and suppresses the formation of rock-salt phases which are unfavorable for  $\text{Li}^+$  transport. Doping can maintain the stability of the material structure and reduce the effect of lattice slippage under high voltage. Doping reduces the activity of the surface lattice oxygen, and inhibits its reaction with the electrolyte components at high temperature. The comparative research further illustrates the mechanism of doping modification on the performance improvement of the SC NCM materials and provides universal experience for the modification of SC NCM materials in the future.

## 2. Results and discussion

### 2.1. Synthesis conditions and material testing

The precursors in this study are obtained by co-precipitation, as shown in Fig. S1a, the NCM811 precursor was spherical secondary particles formed by the accumulation of primary particles. After calcination by the molten salt method, single-crystalline NCM811 materials (SC-NCM811, Fig. S1b) with uniform particles can be prepared with the

precursors. Through the elemental analysis, the elements of nickel, cobalt, and manganese are uniformly distributed in the prepared materials (Fig. S1c). Doping is one of the important methods for the modification of polycrystalline NCM materials. According to literature [28,29], Ti has a good comprehensive effect on the modification of NCM materials. Therefore, Ti is selected as the experimental object of SC NCM modification, and the pre-experiment is carried out with a doping amount of 2 mol%. From the results of SEM (Fig. 1a), the particles of the Ti-doped materials are plump, round and uniform in size. The optimal sintering temperature after doping may be different from the synthesis of the original material, and the doping amount will affect the electrochemical performance of the material to a certain extent. Therefore, on the basis of the pre-experiment, two sets of samples with sintering temperature of 880 °C and 920 °C are added to determine the optimal calcination temperature of the doped material (Fig. S2a). The capacity retention of the pristine SC-NCM811 material after 200 cycles at 3.0–4.3 V at 0.5C is 76.73 %, while that of the doped materials calcined at 880 °C, 900 °C and 920 °C after 200 cycles are 86.89 %, 89.21 % and 87.37 %, respectively. The comparison shows that the slight change of the calcination temperature will not have a significant effect on the properties of the doped material, and the optimal temperature is 900 °C, which is the same as the unmodified sample, so 900 °C is chosen as the calcination temperature of the doped material. The temperature can not only make the material have the optimal electrochemical performance, but also be consistent with the unmodified sample, avoiding the influence of the calcination temperature difference. The choice of doping content has an important influence on the modification of materials. A small amount of doping may have poor modification effect, and a large amount of doping may reduce the electrochemical capacity of the material. Therefore, three doping amounts of 1 mol%, 2 mol%, and 3 mol% are applied for

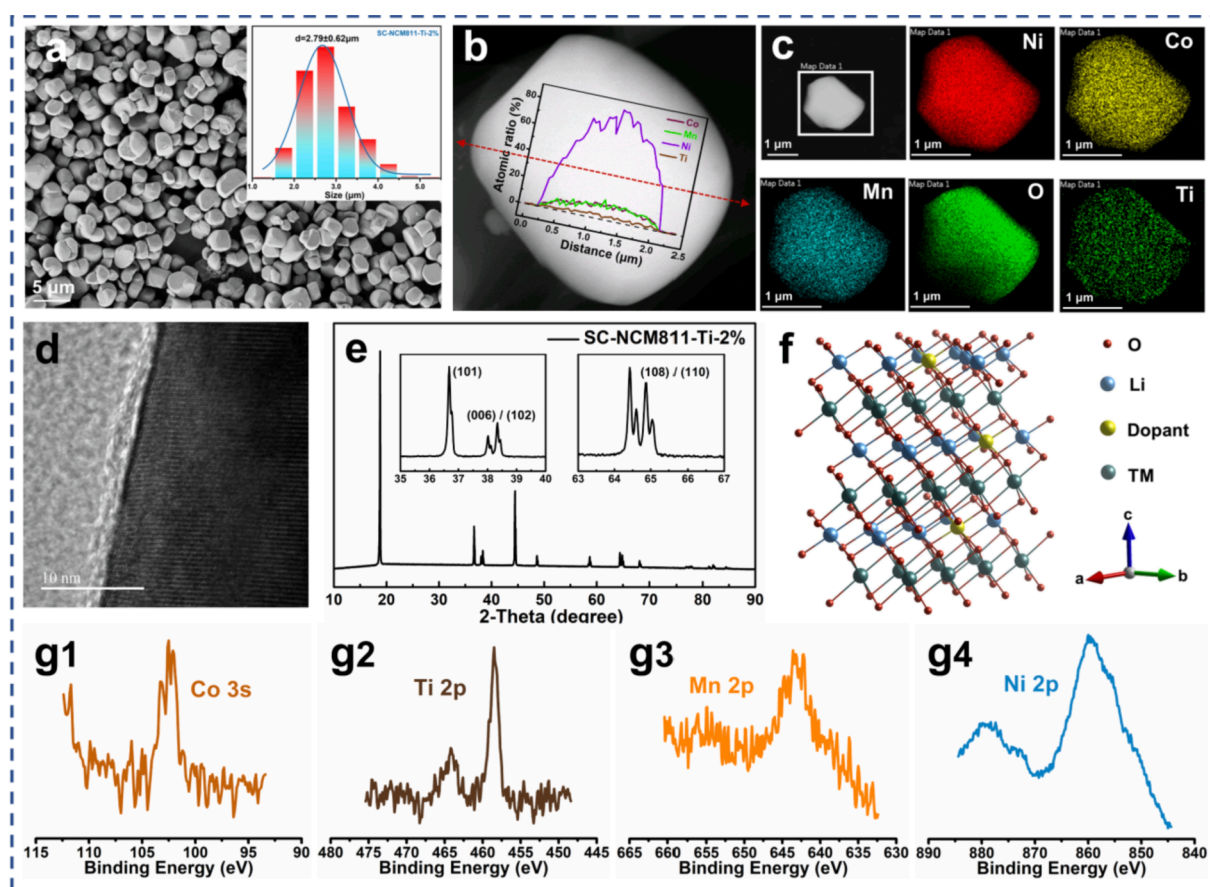


**Fig. 1.** The morphology and particle size of SC-NCM811-Ti-2% material (a), the internal TEM line scan (b) and elemental mapping analysis (c) of the sliced material, the high-resolution TEM (d) and XRD test of the material (e), crystal structure schematic diagram of the material (f), XPS test of the original material (g).



NCM811-Ti-2 % material [31]. These results all indicate that the electrochemical performance of SC NCM811 material has been significantly improved after doping. At the same time, compared with some other research works [22,23,32–38], the performance in this study still shows certain superiority.

In order to clarify the reasons for the improved properties after doping, XRD tests are applied to compare the structural differences between two original materials. The XRD and refined results of SC-NCM811 and SC-NCM811-Ti-2 % materials are shown in Fig. 3a and Fig. 3b respectively. The specific results are shown in the Table S2. Both materials have a good layered structure from the XRD results. For NCM materials, the lower the ratio of the c-axis and the a-axis, the better the structural maintenance of the material [39–41]. The  $c/a$  value of SC-NCM811 material is slightly bigger than that of SC-NCM811-Ti-2 % material, indicating that the latter has stronger structural stability (Table S2). During the cycling process of NCM materials, the (003) crystal plane will shift to a low angle with the extraction of  $\text{Li}^+$  [42], so the XRD results of the two materials after cycling were compared with each other (Fig. 3c), and the peak of Aluminum (Al) is used as the benchmark for correction, the results show that the negative shift of the (003) crystal plane of SC-NCM811 is more obvious than that of SC-NCM811-Ti-2 %. Therefore, the structure of SC-NCM811-Ti-2 % is better preserved after cycling, which is beneficial for better electrochemical performance. Pristine SC-NCM811 (Fig. S3a) and SC-NCM811-Ti-2 % (Fig. S3b) both have a good layered structure from the TEM tests. After 300 cycles, the outer surface area of the SC-NCM811 material almost transforms into rock-salt phase (Fig. 3d), while for the SC-NCM811-Ti-2 % material, the range of rock-salt phase in the outer surface area is about 7–9 nm (Fig. 3e), and the interior still maintains a regular layered

structure, the selected electron diffraction near the surface shows both layered and rock-salt structure. The TEM results show that the SC-NCM811-Ti-2 % can maintain better structural stability in long cycle, and the degree of surface phase transition is significantly reduced, resulting in better electrochemical performance. For the battery with lithium piece as the negative electrode, the transition metal in the NCM materials will dissolve out and deposit on the lithium metal negative electrode during the cycle, which affects the utilization efficiency of lithium metal. The more the transition metal is dissolved out, the thicker the utilization depth of the lithium metal negative electrode is. In the battery with SC-NCM811 materials, the utilization depth of the lithium metal after cycling is about 140–210  $\mu\text{m}$  and uneven (Fig. S4a), while in the battery with SC-NCM811-Ti-2 % materials, the utilization depth of the cycled lithium metal is about 95  $\mu\text{m}$  and relatively uniform (Fig. S4b). From the utilization depth of lithium metal anode, SC-NCM811-Ti-2 % has a low degree of metal dissolution during cycling, so its structure remains relatively intact, which is consistent with the test results of XRD and TEM. In addition to improving the stability of the bulk structure of the material, doping also affects the chemical properties of the surface. The high-nickel NCM material will be accompanied by changes in the oxidation state of the transition metal during the process of  $\text{Li}^+$  deintercalation, which will adversely affect the oxidative decomposition behavior of the electrolyte. After a long cycle of SC-NCM811 materials, a large number of impurities are generated on the surface (Fig. 3f), which are generally considered to be the products of electrolyte decomposition, the impurities are densely distributed, covering almost the entire surface of cathode materials. Although the dispersed impurities can be seen on the surface of cycled SC-NCM811-Ti-2 % (Fig. 3g), the amount is considerably lower than that of SC-NCM811,

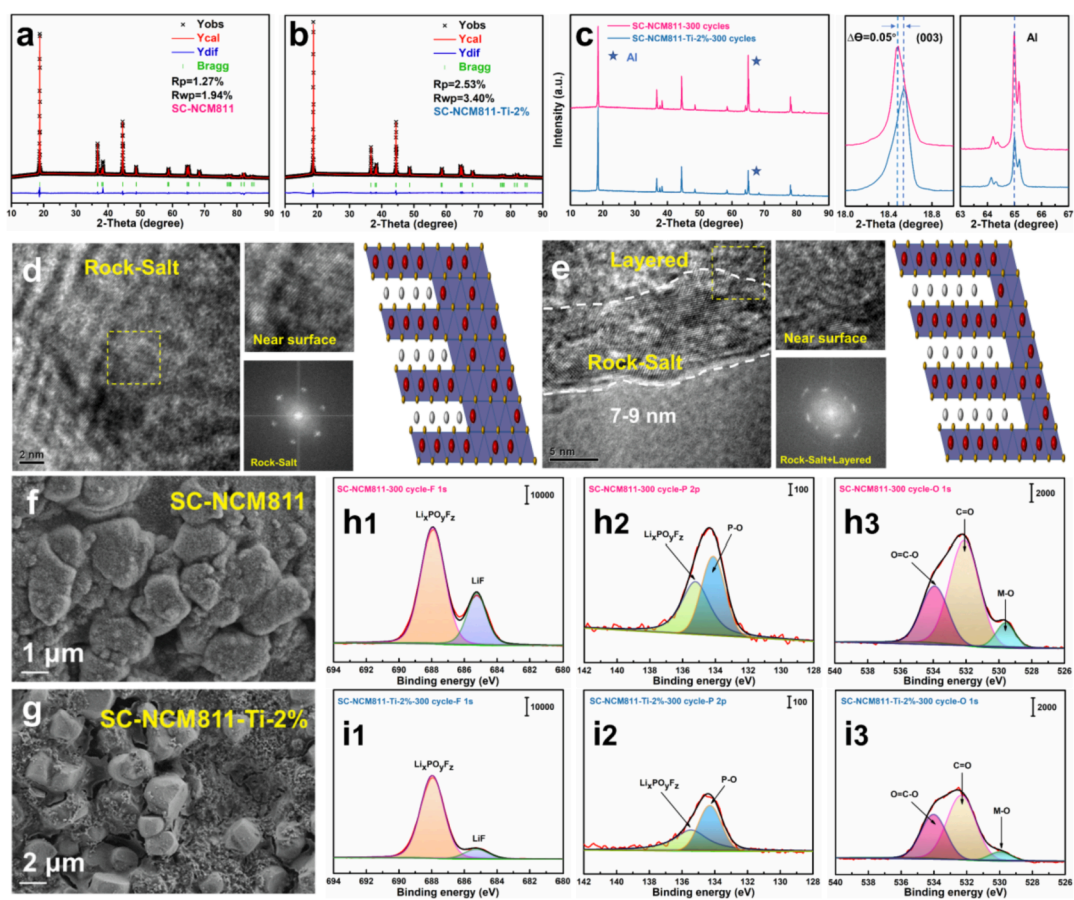


**Fig. 3.** The XRD and refined results of pristine SC-NCM811 (a) and SC-NCM811-Ti-2% (b), XRD results of the two materials after cycling (c), TEM results and schematic diagrams of SC-NCM811 (d) and SC-NCM811-Ti-2% (e) after cycling, SEM results of cycled SC-NCM811 (f) and SC-NCM811-Ti-2% (g), XPS testing of SC-NCM811 (h) and SC-NCM811-Ti-2% (i) after cycling.

and morphology of cathode materials is still clearly visible. It is worth noting that the surfaces of the electrodes composed of the two materials are smooth and neat without any impurities before cycling (Figure S5). When the impurities on the surface of the SC-NCM811 material are impacted with high-energy electrons, the impurity layer will be significantly weakened to expose the bulk material, which further confirms that the surface is a decomposition product of the electrolyte after cycling (Figure S6). The decomposition behavior of the electrolyte on the surface of two materials during the cycle can be observed from XPS tests of cycled electrodes. Peaks at 685.0 eV and 687.5 eV belong to  $\text{LiF}$  and  $\text{Li}_x\text{PF}_y\text{O}_z$  in the F 1s spectrum [43–45]. Peaks at 136.6 eV and 133.5 eV are assigned to the decomposition products  $\text{Li}_x\text{PF}_y$  and  $\text{Li}_x\text{PF}_y\text{O}_z$  for the P 2p spectrum [46]. In the O 1s spectrum, the peaks at 531.91 eV and 533.29 eV correspond to  $\text{C}=\text{O}$  and  $\text{O}-\text{C}=\text{O}$ , respectively [47]. The electrolyte decomposition peak intensity of SC-NCM811 materials (Fig. 3h) after cycling is clearly higher than that of SC-NCM811-Ti-2 % materials (Fig. 3i), which indicates that SC-NCM811 materials undergo more severe electrolyte decomposition during cycling. As the cycle continues, impurities are formed on the surface of electrode materials due to the decomposition of the electrolyte. The components usually have low ionic / electronic conductivity, which will increase the internal resistance of the battery [48]. AC impedance tests are performed on two

kinds of batteries after 300 cycles, the frequency range in the impedance test is  $0.01\text{--}10^5$  Hz. The impedance of cycled SC-NCM811 batteries is significantly larger than that of SC-NCM811-Ti-2 % batteries (Figure S7), which shows that the doping modified material can reduce the decomposition of electrolyte during cycling, and reduce polarization and impedance.

### 2.3. Rate performance analysis

In addition to cycle performance, rate performance is also an important criterion for evaluating NCM materials. Rate performance at 0.2C, 0.5C, 1C, 2C, 5C is performed on SC-NCM811 and SC-NCM811-Ti-2 % materials (Fig. 4a), the performance of two materials is similar at lower rates, while the electrochemical performance of SC-NCM811-Ti-2 % is significantly better than SC-NCM811 at high rates. When cycling at the rate of 2C, the performance decay of SC-NCM811 is more serious than that of SC-NCM811-Ti-2 % (Fig. 4b), which indicates that  $\text{Li}^+$  has a faster transport speed in the SC-NCM811-Ti-2 % material. To find out why SC-NCM811-Ti-2 % has better rate performance, GITT tests are carried out on the materials before and after cycling. The test raw data of the materials before cycling is shown in Figure S8. It can be seen from the Fig. 4c, d that average diffusion coefficients of SC-NCM811 material

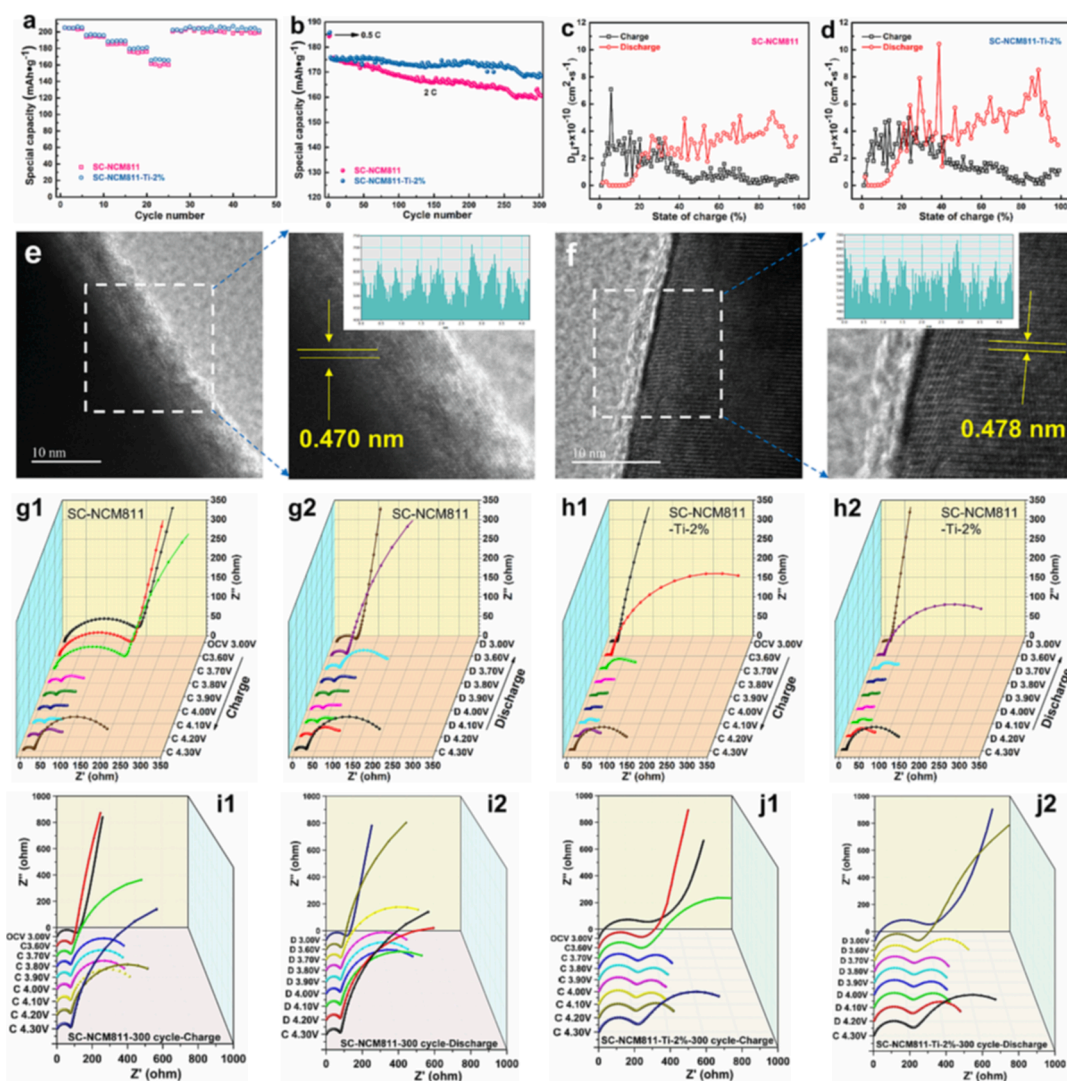


**Fig. 4.** Rate performance (a) and cycle performance test at 2C rate (b) of two materials, diffusion coefficients of uncycled SC-NCM811 (c) and SC-NCM811-Ti-2% (d), high-resolution TEM of pristine SC-NCM811 (e) and SC-NCM811-Ti-2% (f), in-situ impedance of SC-NCM811 (g) and SC-NCM811-Ti-2% (h) before long cycling, in-situ impedance of SC-NCM811 (i) and SC-NCM811-Ti-2% (j) after long cycles.

during charge and discharge are  $1.24 \times 10^{-10}$  ( $\text{cm}^{-2}\cdot\text{s}^{-1}$ ) and  $2.76 \times 10^{-10}$  ( $\text{cm}^{-2}\cdot\text{s}^{-1}$ ), while those of SC-NCM811-Ti-2 % material reach  $1.79 \times 10^{-10}$  ( $\text{cm}^{-2}\cdot\text{s}^{-1}$ ) and  $4.05 \times 10^{-10}$  ( $\text{cm}^{-2}\cdot\text{s}^{-1}$ ), respectively. Therefore, the transport speed of  $\text{Li}^+$  in SC-NCM811-Ti-2 % is higher than that of SC-NCM811 material, showing better rate performance and higher rate cycle performance. At the same time, through the results of high-resolution TEM analysis, the lattice spacing of  $\text{Li}^+$  diffusion layer of SC-NCM811 is 0.470 nm (Fig. 4e), while the lattice spacing of the  $\text{Li}^+$  diffusion layer of SC-NCM811-Ti-2 % reaches 0.478 nm (Fig. 4f), which may be due to the larger radius of the doped Ti ions, increasing the lattice spacing and facilitating the rapid diffusion of  $\text{Li}^+$ . For the material after 300 cycles, the average diffusion coefficients of SC-NCM811 material in the cycle process decrease significantly, which are  $7.39 \times 10^{-11}$  ( $\text{cm}^{-2}\cdot\text{s}^{-1}$ ) and  $4.99 \times 10^{-11}$  ( $\text{cm}^{-2}\cdot\text{s}^{-1}$ ), respectively (Figure S9a). The average diffusion coefficients of cycled SC-NCM811-Ti-2 % material are  $1.35 \times 10^{-10}$  ( $\text{cm}^{-2}\cdot\text{s}^{-1}$ ) and  $7.99 \times 10^{-11}$  ( $\text{cm}^{-2}\cdot\text{s}^{-1}$ ) (Figure S9b), which are also higher than that of the unmodified material. This may be

because the unmodified material has obvious phase transition behavior during the long cycle, and the existence of excessive rock-salt phase seriously hinders the transport of  $\text{Li}^+$ , while the structure of the doped material remains more stable, and there are less rock-salt phases in the material, so the  $\text{Li}^+$  transport speed is faster, which also explains why SC-NCM811-Ti-2 % can have better retention in high-rate cycling. In the process of electrochemical cycling, besides the transport of  $\text{Li}^+$  in the bulk of active materials, its transport performance at the electrode-electrolyte interface also has a great influence on the rate characteristics of the battery. The in-situ impedance tests of the batteries before and after cycling are carried out. The in-situ impedance values of SC-NCM811 and SC-NCM811-Ti-2 % are relatively close before cycling (Fig. 4g, h). While the impedance values of SC-NCM811 material at different potential are significantly higher than SC-NCM811-Ti-2 % after a long cycle (Fig. 4i, j). This is related to the impurities generated on the surface of the SC-NCM811 material during the long cycle, so the cycle performance of the SC-NCM811 material at high rates is significantly

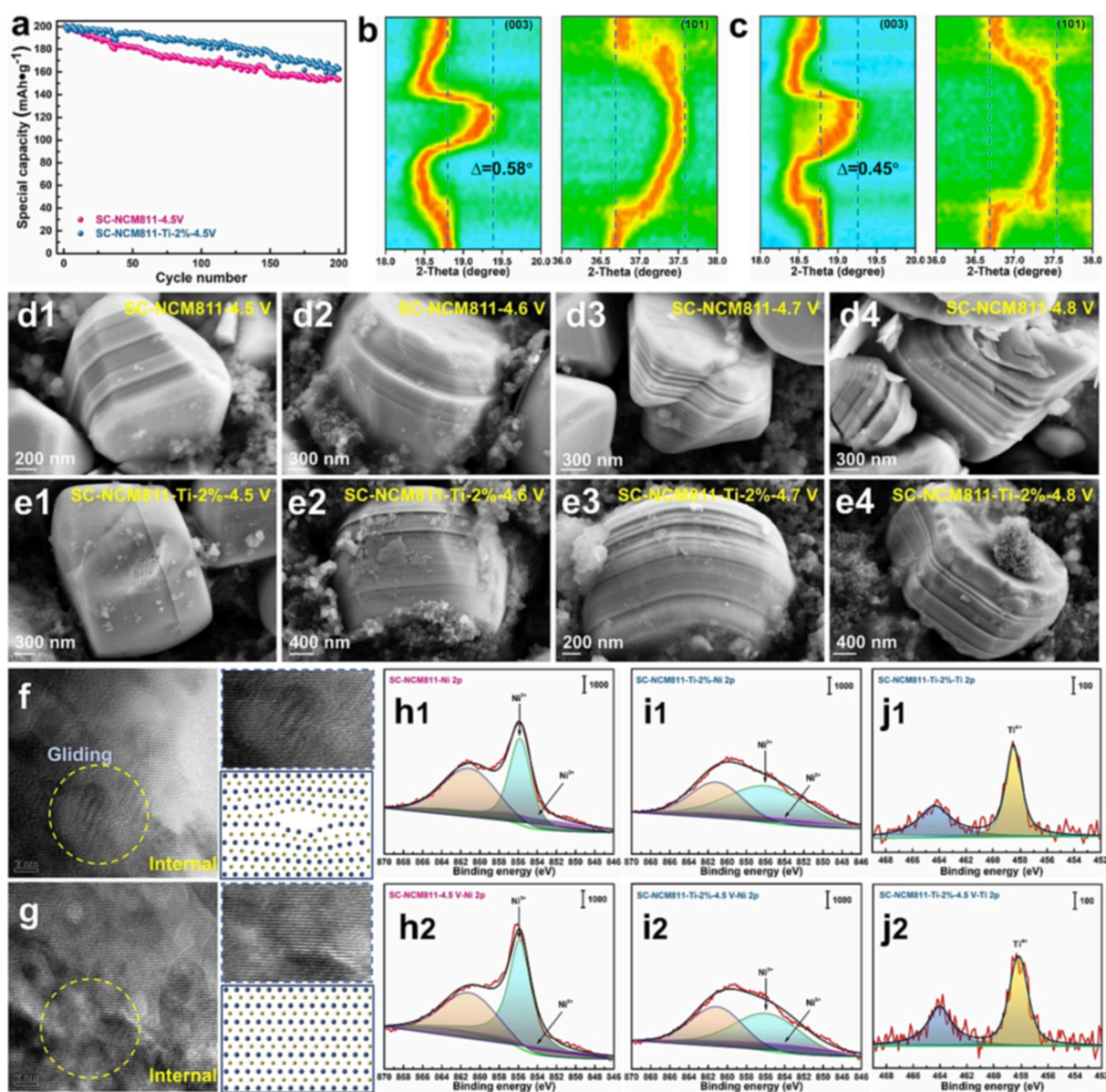


**Fig. 5.** Cycling performance of SC-NCM811 and SC-NCM811-Ti-2 % at 3.0–4.5 V (a), the in-situ XRD test results of SC-NCM811 (b) and SC-NCM811-Ti-2 % (c) at 3.0–4.5 V, SEM images of SC-NCM811 (d) and SC-NCM811-Ti-2 % (e) at different potentials, high-resolution TEM of the interior of SC-NCM811 (f) and SC-NCM811-Ti-2 % (g) after charging to 4.5 V, Ni XPS of SC-NCM811 (h) and SC-NCM811-Ti-2 % (i) before and after charging, Ti XPS of SC-NCM811-Ti-2 % (j) before and after charging.

lower than that of the SC-NCM811-Ti-2 % material.

#### 2.4. High voltage performance analysis

In order to improve the power density of the battery, the working voltage of the NCM battery is also increasing. To investigate the performance and mechanism of doping to enhance the high voltage properties of NCM materials, electrochemical tests on the two materials at 3.0–4.5 V are conducted, respectively. Severe oxidative decomposition will occur when the conventional electrolyte is cycled at high voltage, which greatly affects the electrochemical performance. Therefore, the previously developed high-voltage electrolyte is used for cycling to eliminate the impact of electrolyte degradation on battery performance [15]. The cycling performance of SC-NCM811-Ti-2 % material at 3.0–4.5 V was significantly improved compared with SC-NCM811 (Fig. 5a). The increase in the average voltage of the SC-NCM811 material during charging is higher than that of the SC-NCM811-Ti-2 % material, and the discharge average voltage drop of the SC-NCM811 material is higher than that of the SC-NCM811-Ti-2 % material (Figure S10a, b). Therefore, the average potential difference during cycling under high voltage is more than that of the modified material, and the material polarization is more obvious. Different from the obvious fracture and crushing of polycrystalline NCM under high voltage, single-crystalline NCM will not crack in the crystal gap because there is no secondary particle. However, through the research of Bi, the internal gliding phenomenon of SC NCM will occur under high voltage. Although the lattice gliding will return to its original position after discharge, with the progress of cycle, the gliding will continue to accumulate repeatedly and increase its irreversibility. This phenomenon will lead to the destruction of material structure and the decline of electrochemical performance. For verifying this phenomenon, SC-NCM811 and SC-NCM811-Ti-2 % materials were charged to 4.5 V, 4.6 V, 4.7 V and 4.8 V respectively to observe their gliding behavior under different cut-off voltages. As shown in the Fig. 5d, e, both SC-NCM811 and SC-NCM811-Ti-2 % will slip under high voltage, and the higher the charging voltage is, the more obvious the particle slip is. However, under the same potential, the slip degree of SC-NCM811 material is significantly greater than that of SC-NCM811-Ti-2 % material. SC-NCM811 shows obvious stacking malposition at 4.5 V (Fig. 5d1), while SC-NCM811-Ti-2 % has only slight phenomenon at 4.5 V (Fig. 5e1). When the cut-off voltage is increased to 4.8 V, SC-NCM811 particles break up (Fig. 5d4), and the SC-NCM811-Ti-2 % slippage is deepened, but the intact particle structure is still maintained (Fig. 5e4). SEM tests at different potentials show that doping can well suppress the slip phenomenon of materials at high potential. Through the in-situ XRD tests at 3.0–4.5 V (Fig. 5b, c), the characteristic peaks of SC-NCM811-Ti-2 % have a lower shift at high voltage, especially the shift of the (003) peak (The raw data is shown in Figure S11), which indicates that the volume expansion and contraction during the charging and discharging process are smaller, so the slip is significantly suppressed. High-resolution TEM tests are performed on the sliced materials after charging to 4.5 V to observe the crystal structures on the surface, near surface and interior of the materials under high voltage. The structure of SC-NCM811 at both surface and near-surface regions is transformed into rock-salt phase at 4.5 V, indicating that the material has a relatively obvious transition metal mixing phenomenon with delithiation (Figure S12a). While the SC-NCM811-Ti-2 % material has rock-salt phase in the surface region at 4.5 V, and the near-surface region has the coexistence of rock-salt and layered phase (Figure S12b), the degree of cation mixing is lower than that of the SC-NCM811 material [49]. In the interior of the materials, both of them basically maintain a relatively intact layered structure, but in the SC-NCM811 material (Fig. 5f), obvious diffraction bending can be observed, indicating that metal layer slip occurs inside the material. In the SC-NCM811-Ti-2 % material (Fig. 5g), the internal structure is intact and no obvious bending phenomenon is observed. The TEM results can also prove that doping can

well suppress the slip of the SC NCM material under high voltage. At the same time, XPS tests on both materials are also operated before and after charging to 4.5 V. For the SC-NCM811 material, the Ni oxidation state on the surface changes significantly after charging, the proportion of  $\text{Ni}^{2+}$  decreases significantly, while the proportion of  $\text{Ni}^{3+}$  increases (Fig. 5h1, h2). For SC-NCM811-Ti-2 %, the XPS results of Ti are almost identical before and after charging, indicating that there is no valence change (Fig. 5j1, j2). Due to the existence of Ti, the valence state of Ni in SC-NCM811-Ti-2 % is also relatively stable before and after charging (Fig. 5i1, i2). It shows that the valence of the doped Ti does not change during the electrochemical process, which plays a role in stabilizing the structure. Therefore, the lattice slip degree of SC-NCM811-Ti-2 % material under high voltage is lower than that of SC-NCM811.

#### 2.5. Thermal stability analysis

The thermal stability of high-nickel NCM materials is a key factor which plagues their practical use, so the effect of doping modification on the thermal stability of SC NCM materials is worth exploring. Oxygen release of delithiated NCM materials will occur at high temperature, the carbonate solvent dehydrogenates and adsorbs on the lattice oxygen on the surface of the NCM material with high oxidation state, the influence of dual effect greatly reduces the thermal stability of the charged NCM materials. DSC tests on SC-NCM811 and SC-NCM811-Ti-2 % charged to 4.3 V are performed, respectively (Fig. 6a), and the SC-NCM811 material would preferentially undergo exothermic phenomena accompanied by mass loss and oxygen release. In order to find out the structure change process of the NCM materials at high temperature, in-situ Raman tests on the two materials charged to 4.3 V are conducted. The test results were normalized by the intensity of the  $E_g$  peak and displayed in the form of a contour plot. During the in-situ heating Raman process, with the increase of temperature, the material will undergo layered transformation to spinel and rock-salt phase, and the intensity of  $A_{1g}$  and  $E_g$  peaks will gradually weaken. In the Fig. 6b, c, the phase transition temperature of the SC-NCM811 material is lower than that of the SC-NCM811-Ti-2 % material, so the metal–oxygen bonding force in the material is also weaker at the same temperature, and the thermal stability of SC-NCM811 material is lower than that of SC-NCM811-Ti-2 % material. In practical batteries, the electrode materials often coexist with the electrolyte, so DSC tests on the charged NCM materials are conducted in the presence of electrolyte. The exothermic intensity in the DSC test with electrolyte is significantly higher than that of the material powder only, but the initial exothermic temperature of the reaction between the delithiated SC-NCM811 material and the electrolyte is also lower than that of the SC-NCM811-Ti-2 % material, and the heat release is also slightly higher (Fig. 6d). In our previous research [50], the carbonate solvent will undergo a dehydrogenation reaction on the surface of the delithiated high-nickel NCM materials, and then adsorb on the surface lattice oxygen and be further oxidized by it, thereby accelerating the thermal reaction process. From the results of in-situ heating Raman, at high temperature, due to the presence of doped metal Ti, the metal–oxygen binding force in the NCM material is enhanced, and the activity of surface lattice oxygen in the material is reduced. Therefore, the activity of the electrolyte solvent to react with the surface of the material is reduced, and the thermal stability of the material is improved. At the same time, the oxygen vacancy formation energy of the doped NCM is higher than that of the original material [51], and it is less likely for the doped NCM to release oxygen after delithiation, so the degree of reaction with the electrolyte is also significantly reduced.

### 3. Conclusions

In this work, the SC high-nickel NCM811 is modified by doping with Ti element. The stabilizing effect of Ti can enhance the structural stability of SC NCM811 during the electrochemical process, and due to the weakening of the metal dissolution phenomenon in the NCM material,

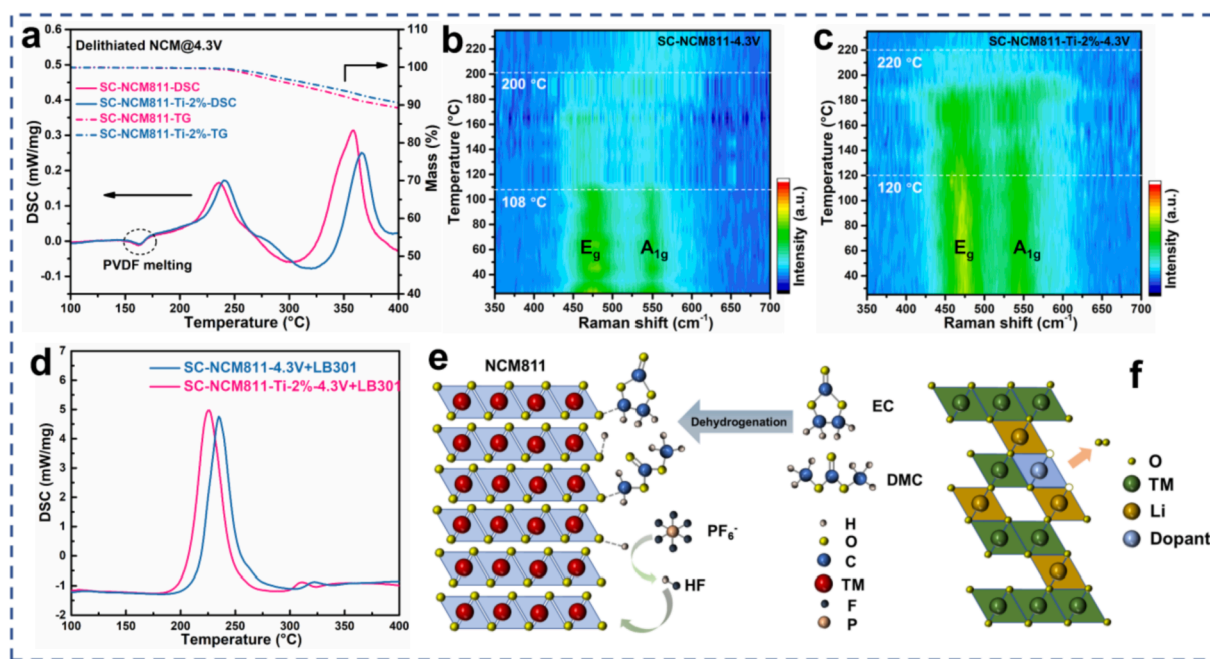


**Fig. 6.** TG-DSC test of delithiated NCM materials (a), in-situ heating Raman tests of charged SC-NCM811 (b) and SC-NCM811-Ti-2% (c), delithiated NCM materials DSC tests with electrolyte (d), schematic diagram of the reaction of electrolyte with NCM materials (e) and oxygen vacancy formation (f).

the utilization efficiency of lithium metal anode is improved. The valence state of the doped Ti element is stable, which reduces the decomposition effect of high-valent Ni on the electrolyte and reduces the generation of surface impurities. Therefore, doping can significantly improve the cycle performance of SC NCM811 materials. The rate capability of the SC NCM811 is improved because Ti with a larger radius increases the interlayer spacing for Li<sup>+</sup> diffusion and suppresses the formation of rock-salt phases which are unfavorable for Li<sup>+</sup> transport. When cycling at a higher potential, the valence state of NCM transition metals will change accordingly, while Ti still maintains a stable valence state. Therefore, doping can maintain the stability of the material structure and reduce the effect of lattice slippage, which can improve the high-voltage performance of the material. At the same time, the doped Ti can reduce the oxygen release of the delithiated material at high temperature, reduce the activity of the surface lattice oxygen, and inhibit its reaction with the electrolyte components, thereby increasing the thermal stability of the NCM material. This work researches the effect of metal doping on the performance of single-crystalline high-nickel NCM materials and provides convincing mechanism explanation, which supplies a reference for the further modification of SC NCM materials.

## 4. Experimental section

### 4.1. Precursor synthesis by co-precipitation method

The precursors for the preparation of the SC NCM material by the molten-salt method were obtained by co-precipitation routine. The stoichiometric ratio (8:1:1) of NiSO<sub>4</sub>·6H<sub>2</sub>O, CoSO<sub>4</sub>·7H<sub>2</sub>O and MnSO<sub>4</sub>·H<sub>2</sub>O was prepared into a mixed salt solution (MSO<sub>4</sub>) with a total concentration of 2 mol·L<sup>-1</sup>, and then 2 mol·L<sup>-1</sup> NaOH solution was used as the co-precipitation alkali source. During the experiment, the ammonia solution was prepared according to the ratio of NH<sub>3</sub>·H<sub>2</sub>O:MSO<sub>4</sub> = 0.2 and added dropwise with NaOH and mixed salt solution at the same time during the co-precipitation process. The pH value of the solution was kept constant at 11.5. At the same time, the solution system temperature was 55 °C, the stirring speed was 750 rpm, and the inert gas was continuously fed. After the injection procedure was completed, the constant temperature was maintained for 12 h.

### 4.2. Synthesis of single-crystalline NCM materials

The SC NCM materials were synthesized by the molten-salt method. The precursors, LiOH·H<sub>2</sub>O and Li<sub>2</sub>SO<sub>4</sub>·H<sub>2</sub>O in a stoichiometric ratio (2:3:5) were ground and mixed, respectively. The mixture was pre-calcined at 500 °C for 3 h in oxygen atmosphere, and then calcined at 900 °C for 10 h. The calcined materials were washed with deionized water to remove excess lithium salts, and then recalcined at 650 °C under oxygen atmosphere for 6 h. The preparation of doped SC NCM materials requires adding the desired proportion of dopant material during the grinding process.

### 4.3. Electrode preparation and battery assembly

In the process of positive electrode preparation, the mass ratio of active material, conductive agent and binder is 8: 1: 1, and a proper amount of *N*-Methylpyrrolidone (NMP) was added into the powder to make the slurry. The whole material was put into the agitating defoamer for stirring and mixing. After that, it was uniformly coated on the aluminum foil current collector, dried in a vacuum oven at 80 °C for 24 h, and then the electrode was punched into a circular sheet with a diameter of 12 mm, in addition, the mass loading of positive electrodes is about 8 mg·cm<sup>-2</sup>. In the battery assembly process, the obtained electrode pieces were positive electrodes, and the lithium pieces were negative electrodes. The LB-301 electrolyte (EC: DMC = 1: 1 (v: v), 1 M LiPF<sub>6</sub>) and the Asahi Kasei separator were used respectively.

### 4.4. Electrochemical performance test

The batteries were tested by Neware battery test system, and the programs were set according to the test requirements. To study the lithium-ion diffusion coefficients of materials in the cycling process, the galvanostatic intermittent titration technique (GITT) was applied. In addition, the electrochemical workstation Autolab was applied to test the in-situ impedance of the batteries, and the Solartron was used to test the battery impedance of different cycles.

#### 4.5. Physical characterization

In this study, XRD was used to test the structural properties of the materials, TEM was used to observe the structural changes of the materials in different states, XPS was applied to analyze the decomposition products on the surface of the materials after cycling and the valence state change of the materials in the charged state, SEM was functioned to monitor the overall morphology and particle size of the materials, DSC was employed to investigate the thermal stability of the materials under delithiation, and Raman was used to measure the change of cathode materials with temperature after delithiation.

#### Declaration of Competing Interest

The authors declare that they have no known competing financial interests or personal relationships that could have appeared to influence the work reported in this paper.

#### Data availability

The data that has been used is confidential.

#### Acknowledgements

We gratefully acknowledge the financial support of National Key Research and Development Program of China (2017YFB0102000), the Key Project of Science and Technology of Xiamen (3502Z20201013), National Natural Science Foundation of China (21875198, 21875195, 22021001). We are very grateful to Professor Yu Qiao for his help during the experiment. We also acknowledge the help of Tan Kah Kee Innovation Laboratory on the scientific tests.

#### Appendix A. Supplementary data

Supplementary data to this article can be found online at <https://doi.org/10.1016/j.cej.2022.139431>.

#### References

- M. Neaimeh, G.A. Hill, Y. Hübner, et al., Routing systems to extend the driving range of electric vehicles, *IET Intell Transp Sy* 7 (3) (2013) 327–336.
- S. Kim, J. Lee, C. Lee, Does Driving Range of Electric Vehicles Influence Electric Vehicle Adoption? *Sustainability* 9 (10) (2017).
- W. Kempton, Electric vehicles: Driving range, *Nat Energy* 1 (9) (2016) 16131.
- X. Zuo, J. Zhu, P. Müller-Buschbaum, et al., Silicon based lithium-ion battery anodes: A chronicle perspective review, *Nano Energy* 31 (2017) 113–143.
- X. Su, Q. Wu, J. Li, et al., Silicon-Based Nanomaterials for Lithium-Ion Batteries: A Review, *Adv Energy Mater* 4 (1) (2014) 1300882.
- Y. Mekonnen, A. Sundararajan, A.I. Sarwat. A review of cathode and anode materials for lithium-ion batteries; proceedings of the SoutheastCon 2016, F 30 March-3 April 2016, 2016 [C].
- A. Manthiram, A reflection on lithium-ion battery cathode chemistry, *Nat Commun* 11 (1) (2020) 1550.
- U. Nisar, N. Muralidharan, R. Essehli, et al., Valuation of Surface Coatings in High-Energy Density Lithium-ion Battery Cathode Materials, *Energy Stor Mater* 38 (2021) 309–328.
- S. Jamil, G. Wang, M. Fasehullah, et al., Challenges and prospects of nickel-rich layered oxide cathode material, *J Alloys Compd* 909 (2022), 164727.
- Y.J. Bi, W.C. Yang, R. Du, et al. Correlation of oxygen non-stoichiometry to the instabilities and electrochemical performance of LiNi<sub>0.8</sub>Co<sub>0.1</sub>Mn<sub>0.1</sub>O<sub>2</sub> utilized in lithium ion battery, *J Power Sources*, 283(2015), 211–218.
- S.-M. Bak, E. Hu, Y. Zhou, et al., Structural Changes and Thermal Stability of Charged LiNi<sub>x</sub>Mn<sub>y</sub>Co<sub>z</sub>O<sub>2</sub> Cathode Materials Studied by Combined In Situ Time-Resolved XRD and Mass Spectroscopy, *ACS Appl Mater Interfaces* 6 (24) (2014) 22594–22601.
- C.S. Yoon, K.-J. Park, U.-H. Kim, et al., High-Energy Ni-Rich Li[Ni<sub>x</sub>Co<sub>y</sub>Mn<sub>1-x-y</sub>]O<sub>2</sub> Cathodes via Compositional Partitioning for Next-Generation Electric Vehicles, *Chem Mater* 29 (24) (2017) 10436–10445.
- K.-J. Park, H.-G. Jung, L.-Y. Kuo, et al., Improved Cycling Stability of Li[Ni<sub>0.90</sub>Co<sub>0.05</sub>Mn<sub>0.05</sub>]O<sub>2</sub> Through Microstructure Modification by Boron Doping for Li-Ion Batteries, *Adv Energy Mater* 8 (25) (2018) 1801202.
- Y. Zhang, Z.-B. Wang, F.-D. Yu, et al. Studies on stability and capacity for long-life cycle performance of Li(Ni<sub>0.5</sub>Co<sub>0.2</sub>Mn<sub>0.3</sub>)O<sub>2</sub> by Mo modification for lithium-ion battery, *J Power Sources*, 358(2017), 1–12.
- X. Kong, J. Liu, Y. Zhang, et al. An effective electrolyte design to improve the high-voltage performance of high-capacity NCM811/SiO<sub>x</sub>-Gr batteries, *Electrochim Acta*, 349(2020), 136356.
- S. Jamil, G. Wang, L. Yang, et al., Suppressing H<sub>2</sub>-H<sub>3</sub> phase transition in high Ni-low Co layered oxide cathode material by dual modification, *J Mater Chem A* 8 (40) (2020) 21306–21316.
- M. Hong-yun, Y. Xiao-hui, M. Meng-yao, et al. Degradation Mechanism of LiNi<sub>0.83</sub>Co<sub>0.12</sub>Mn<sub>0.05</sub>O<sub>2</sub> Cycled at 45 °C, *J Electrochem*, 26(3), (2020), 431.
- S.-N.-G. Jia-Yi Wang, X. Wang, Lin Gu, Dong Su. Structural Degradation of Ni-Rich Layered Oxide Cathode for Li-Ion Batteries, *J Electrochem* 28 (2) (2022) 2108431.
- X. Kong, Y. Zhang, S. Peng, et al., Superiority of Single-Crystal to Polycrystalline LiNi<sub>x</sub>Co<sub>y</sub>Mn<sub>1-x-y</sub>O<sub>2</sub> Cathode Materials in Storage Behaviors for Lithium-Ion Batteries, *ACS Sustainable Chem Eng* 8 (39) (2020) 14938–14948.
- X. Kong, Y. Zhang, J. Li, et al., Single-crystal structure helps enhance the thermal performance of Ni-rich layered cathode materials for lithium-ion batteries, *Chem Eng J* 434 (2022), 134638.
- E. Trevisanello, R. Ruess, G. Conforto, et al., Polycrystalline and Single Crystalline NCM Cathode Materials—Quantifying Particle Cracking, Active Surface Area, and Lithium Diffusion, *Adv Energy Mater* 11 (18) (2021) 2003400.
- X. Fan, G. Hu, B. Zhang, et al., Crack-free single-crystalline Ni-rich layered NCM cathode enable superior cycling performance of lithium-ion batteries, *Nano Energy* 70 (2020), 104450.
- X. Ma, P. Vanaphuti, J. Fu, et al., A universal etching method for synthesizing high-performance single crystal cathode materials, *Nano Energy* 87 (2021), 106194.
- L. Zheng, J.C. Bennett, M.N. Obrovac, All-Dry Synthesis of Single Crystal NMC Cathode Materials for Li-Ion Batteries, *J Electrochem Soc* 167 (13) (2020), 130536.
- Y. Han, Y. Lei, J. Ni, et al. Single-Crystalline Cathodes for Advanced Li-Ion Batteries: Progress and Challenges, Small, n/a(n/a), (2022), 2107048.
- S. Jamil, A. Bin Yousaf, S. Hee Yoon, et al. Dual cationic modified high Ni-low co layered oxide cathode with a heteroepitaxial interface for high energy-density lithium-ion batteries, *Chem Eng J*, 416(2021), 129118.
- W. Yao, Y. Liu, D. Li, et al., Synergistically Enhanced Electrochemical Performance of Ni-rich Cathode Materials for Lithium-ion Batteries by K and Ti Co-modification, *J Phys Chem C* 124 (4) (2020) 2346–2356.
- Y. Cheng, Y. Sun, C.T. Chu, et al., Stabilizing effects of atomic Ti doping on high-voltage high-nickel layered oxide cathode for lithium-ion rechargeable batteries, *Nano Res* (2022).
- X. Zhang, Y. Qiu, F. Cheng, et al., Realization of a High-Voltage and High-Rate Nickel-Rich NCM Cathode Material for LIBs by Co and Ti Dual Modification, *ACS Appl Mater Interfaces* 13 (15) (2021) 17707–17716.
- F. Cheng, X. Zhang, Y. Qiu, et al., Tailoring electrolyte to enable high-rate and super-stable Ni-rich NCM cathode materials for Li-ion batteries, *Nano Energy* 88 (2021), 106301.
- Y. Bi, J. Tao, Y. Wu, et al., Reversible planar gliding and microcracking in a single-crystalline Ni-rich cathode, *Science* 370 (6522) (2020) 1313.
- A. Ran, S. Chen, M. Cheng, et al., Single-crystal nickel-rich material as a highly stable cathode for lithium-ion batteries, *J Mater Chem A* (2022).
- F. Zhang, S. Lou, S. Li, et al., Surface regulation enables high stability of single-crystal lithium-ion cathodes at high voltage, *Nat Commun* 11 (1) (2020) 3050.
- H.-H. Ryu, B. Namkoong, J.-H. Kim, et al., Capacity Fading Mechanisms in Ni-Rich Single-Crystal NCM Cathodes, *ACS Energy Lett* 6 (8) (2021) 2726–2734.
- Y.G. Zou, H. Mao, X.H. Meng, et al., Mitigating the Kinetic Hindrance of Single-Crystalline Ni-Rich Cathode via Surface Gradient Penetration of Tantalum, *Angew Chem, Int Ed Engl* 60 (51) (2021) 26535–26539.
- Y. Han, S. Heng, Y. Wang, et al., Anchoring Interfacial Nickel Cations on Single-Crystal LiNi<sub>0.8</sub>Co<sub>0.1</sub>Mn<sub>0.1</sub>O<sub>2</sub> Cathode Surface via Controllable Electron Transfer, *ACS Energy Lett* 5 (7) (2020) 2421–2433.
- J. Zhu, J. Zheng, G. Cao, et al. Flux-free synthesis of single-crystal LiNi<sub>0.8</sub>Co<sub>0.1</sub>Mn<sub>0.1</sub>O<sub>2</sub> boosts its electrochemical performance in lithium batteries, *J Power Sources*, 464(2020).
- Z. Feng, R. Rajagopalan, S. Zhang, et al., A Three in One Strategy to Achieve Zirconium Doping, Boron Doping, and Interfacial Coating for Stable LiNi<sub>0.8</sub>Co<sub>0.1</sub>Mn<sub>0.1</sub>O<sub>2</sub> Cathode, *Adv Sci* 8 (2) (2021) 2001809.
- I. Buchberger, S. Seidlmayer, A. Pokharel, et al. Aging Analysis of Graphite/LiNi<sub>1/3</sub>Mn<sub>1/3</sub>Co<sub>1/3</sub>O<sub>2</sub> Cells Using XRD, PGAA, and AC Impedance, *J Electrochem Soc*, 162(14), (2015), A2737-A2746.
- P.-H. Lee, S.-H. Wu, W.K. Pang, et al., The storage degradation of an 18650 commercial cell studied using neutron powder diffraction, *J Power Sources* 374 (2018) 31–39.
- A. Iturrondobeitia, F. Aguesse, S. Genies, et al., Post-Mortem Analysis of Calendar-Aged 16 Ah NMC/Graphite Pouch Cells for EV Application, *J Phys Chem C* 121 (40) (2017) 21865–21876.
- X.B. Kong, S.Y. Peng, J.Y. Li, et al. Pre-blended conductive agent to effectively improve the storage properties of LiNi<sub>0.6</sub>Co<sub>0.2</sub>Mn<sub>0.2</sub>O<sub>2</sub> cathode materials, *J Power Sources*, 448(2020), 227445.
- A.S. Wotango, W.N. Su, E.G. Leggesse, et al., Improved Interfacial Properties of MCMB Electrode by 1-(Trimethylsilyl)imidazole as New Electrolyte Additive To Suppress LiPF<sub>6</sub> Decomposition, *ACS Appl Mater Interfaces* 9 (3) (2017) 2410–2420.
- H. Cai, H. Jing, X. Zhang, et al. Improving High-Voltage Performance of Lithium-Ion Batteries with Sulfolane as an Electrolyte Additive, *J Electrochem Soc*, 164(4), (2017), A714-A720.
- Y. Liu, X. Fan, B. Luo, et al., Understanding the enhancement effect of boron doping on the electrochemical performance of single-crystalline Ni-rich cathode materials, *J. Colloid Interface Sci.* 604 (2021) 776–784.

- [46] H.B. Rong, M.Q. Xu, Y.M. Zhu, et al., A novel imidazole-based electrolyte additive for improved electrochemical performance of high voltage nickel-rich cathode coupled with graphite anode lithium ion battery, *J Power Sources* 332 (2016) 312–321.
- [47] S. Lin, H. Hua, P. Lai, et al., A multifunctional dual-salt localized high-concentration electrolyte for fast dynamic high-voltage lithium battery in wide temperature range, *Adv Energy Mater* 11 (36) (2021) 2101775.
- [48] X.B. Kong, R. Zhou, J. Wang, et al., An effective electrolyte strategy to improve the high-voltage performance of LiCoO<sub>2</sub> cathode materials, *ACS Appl Energy Mater* 2 (7) (2019) 4683–4691.
- [49] Z. Tang, Z. Feng, D. Deng, et al. Optimization of Sr-doping boosting the structural stability for single crystalline LiNi<sub>0.8</sub>Co<sub>0.1</sub>Mn<sub>0.1</sub>O<sub>2</sub> cathode to enhance its electrochemical performance at elevated voltage and temperature, *J Power Sources*, 545(2022), 231915.
- [50] J. Li, H. Hua, X. Kong, et al., In-situ probing the near-surface structural thermal stability of high-nickel layered cathode materials, *Energy Stor Mater* 46 (2022) 90–99.
- [51] D.H. Kim, J.H. Song, C.H. Jung, et al., Stepwise dopant selection process for high-nickel layered oxide cathodes, *Adv Energy Mater* 12 (18) (2022) 2200136.